Journal of Nuclear Materials 452 (2014) 57–60

Contents lists available at ScienceDirect

Journal of Nuclear Materials

journal homepage: www.elsevier.com/locate/jnucmat

He implantation of bulk Cu–Nb nanocomposites fabricated by accumulated roll bonding

W.Z. Han [a,b,*], N.A. Mara [b], Y.Q. Wang [c], A. Misra [b], M.J. Demkowicz [d]

[a] Center for Advancing Materials Performance from the Nanoscale, State Key Laboratory for Mechanical Behavior of Materials, Xi'an Jiaotong University, Xi'an 710049, PR China
[b] Center for Integrated Nanotechnologies, Los Alamos National Laboratory, Los Alamos, NM 87545, USA
[c] Materials Science and Technology Division, Los Alamos National Laboratory, Los Alamos, NM 87545, USA
[d] Department of Materials Science and Engineering, Massachusetts Institute of Technology, Cambridge, MA 02139, USA

ARTICLE INFO

Article history:
Received 16 February 2014
Accepted 23 April 2014
Available online 9 May 2014

ABSTRACT

We perform room temperature and elevated temperature He implantation of bulk Cu–Nb nanocomposites synthesized by accumulated roll bonding (ARB). Transmission electron microscopy (TEM) reveals that nanoscale He precipitates form preferentially along Cu-Nb interfaces during implantation at 20 °C and 450 °C. Bubble-free zones may be identified near interfaces after implantation at 450 °C. He implantation at 480 °C results in large, faceted cavities in thick Cu layers and highly elongated cavities in thin Cu layers. Only nanoscale bubbles are seen in Nb layers after implantation at 480 °C. Similar to vapor deposited Cu–Nb multilayers, ARB Cu–Nb nanocomposites exhibit He precipitate morphologies that are highly sensitive to implantation temperature and layer thickness.

1. Introduction

Extensive studies have been conducted on the effect of He implantation on several types of physical vapor deposited (PVD) multilayers, including Cu–Nb [1–7], Cu–V [8,9], Cu–Mo [10], and Ag–V [11]. Studies on these model systems have led to considerable insight into the mechanisms of He interaction with microstructural features in heterophase composites. They have shown that interfaces between successive layers are preferential sites for trapping He and that He bubbles form at these interfaces only after a critical interfacial He concentration has been exceeded [4,9–14]. This behavior has been explained in terms of interface structure through multiscale modeling [15,16]. These studies also elucidated the interplay between microstructure and He-induced hardening [17].

Recently, bulk Cu–Nb nanocomposites have been fabricated using accumulative roll bonding (ARB) [18–22]. Similar to PVD Cu–Nb composites, ARB Cu–Nb has a layered morphology. However, ARB Cu–Nb composites contain different types of predominant interfaces than in PVD Cu–Nb, for example ones where Cu{112} and Nb {112} planes meet and $a\langle 110\rangle$ direction in the Cu interface plane is parallel to $a\langle 111\rangle$ direction in the Nb interface plane [18–22]. Furthermore, unlike magnetron sputtered composites, which may only be synthesized in relatively small quantities, ARB Cu–Nb nanocomposites may be fabricated in bulk [20], making them amenable to large-scale industrial use. Bulk ARB Cu–Nb nanocomposites have already proven to be exceptionally strong, thermally stable [18,21], and resistant to light ion irradiation [18]due to the interfaces they contain. In the present work, we examined the response of ARB Cu–Nb nanocomposites to He implantation at room temperature and elevated temperatures.

2. Experimental procedures

ARB Cu–Nb composites of varying layer thicknesses were fabricated using a combination of rolling reduction, cleaning, cutting, stacking, and further rolling [18,22]. The process began with one plate of polycrystalline reactor grade Nb (99.97% purity) and two plates of oxygen-free high conductivity Cu (99.99% purity) with a thickness of 1 mm and 0.5 mm respectively, length of 20 cm, and width of 6.5 cm. To promote bonding, the surfaces were cleaned ultrasonically for five-min in an acetone bath followed by wire brushing. Roll bonding was performed at room temperature with a ~50% reduction in thickness. Here, we studied ARB Cu–Nb with average layer thickness of 20 nm: close to the lower limit of layer thickness that may be fabricated. He implantation was conducted using an ion energy of 200 keV to a dose of 2×10^{21} ions/m^2 with the ion flux rate of 2.8×10^{-4} dpa/s at three different temperatures: 20 °C, 450 °C and 480 °C. He elevated temperatures were chosen to compare our results with two previous studies: one that

* Corresponding author at: Center for Advancing Materials Performance from the Nanoscale, State Key Laboratory for Mechanical Behavior of Materials, Xi'an Jiaotong University, Xi'an 710049, PR China. Tel.: +86 2982664630.
E-mail address: wzhanmail@gmail.com (W.Z. Han).

http://dx.doi.org/10.1016/j.jnucmat.2014.04.034
0022-3115/

investigates light ion irradiation in ARB Cu–Nb composites [18] and another that studies high temperature He implantation in sputter deposited Cu–Nb composites [5]. Before He implantation, the top surface of the ARB Cu–Nb plate was polished to mirror quality. After implantation, cross-section transmission electron microscopy (XTEM) foils were prepared and then examined using a Tecnai F30 operated at 300 keV with a field emission gun. Implantation damage was examined using through-focal imaging with defocus of ±1 μm or ±3 μm.

3. Results and discussion

Variations of displacement damage and implanted He concentration with depth from the surface were calculated using SRIM and are shown in Fig. 1(a). The peak He concentration of ~15 at.% is found at a depth of ~550 nm. The corresponding damage is ~20 dpa. The peak implanted depth is ~900 nm. Fig. 1(b) shows a corresponding TEM micrograph of a ARB Cu–Nb nanocomposite He implanted at 20 °C. Nanoscale He precipitates may be identified as white dots across the entire He implanted region. They are most numerous in the region with highest implanted He concentration (450–650 nm). Fewer He bubbles are seen near the sample surface and at the end of implanted region.

Figs. 2–4 illustrate He-induced microstructures in the peak He concentration region in ARB Cu–Nb implanted with He at different temperatures. After implantation at 20 °C, numerous nanoscale He bubbles approximately 2 nm in diameter are found in both Cu and Nb layers, as shown in Fig. 2. More bubbles form along Cu–Nb interfaces than within either crystalline layer, indicating that interfaces are preferential He trapping sites. Fig. 3(a) shows that after 450 °C implantation, the distribution of He bubbles is similar to the 20 °C case. However, while He bubble diameters in Nb remain in the ~2 nm range, in Cu they are noticeably larger, at ~5 nm. Interfacial bubbles are larger still, approaching widths of ~7 nm. They tend to be elliptical in shape and grow preferentially into the Cu layer due to the lower vacancy formation energy there [15].

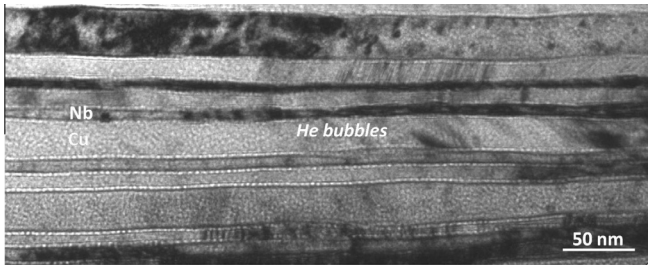

Fig. 2. XTEM image, −1 μm defocus, of the region with peak He concentration in ARB Cu–Nb composites implanted with He at 20 °C.

Narrow bubble-free zones, such as those marked in Fig. 3(a) and highlighted in Fig. 3(b) and (c), may be identified near Cu–Nb interfaces in ARB composites implanted at 450 °C. These zones arise due to the preferential trapping of He at interfaces as well as the higher mobility of He, vacancies, and He-vacancy complexes at 450 °C, compared to 20 °C. Interfacial He bubbles that grow into a thin Cu layer from opposite sides may become sufficiently large to coalesce, as shown in Fig. 3(d). He bubble coalescence does not lead to breakdown of the layered morphology of the composites.

He-induced microstructures created during implantation at 480 °C, shown in Fig. 4(a), differ dramatically from those in 20 °C and 450 °C implantations. Numerous faceted cavities with ~20 nm diameters are seen in thicker Cu layers. These cavities tend to be located near Cu–Nb interfaces, but are not always overlapping with them. Cavities filled with He at high pressure are usually spherical because this shape has minimum surface area for a given volume. The cavities in Fig. 4(a) are faceted because they contain low pressure He gas. Thus, these cavities are likely He-filled voids, rather than He bubbles, and may have formed through a "bubble-to-void" transition [25,26]. He-filled voids of such shape were only observed at higher temperatures in previous investigations carried out on He implanted Cu and Cu–B alloys [23,24]. There are several

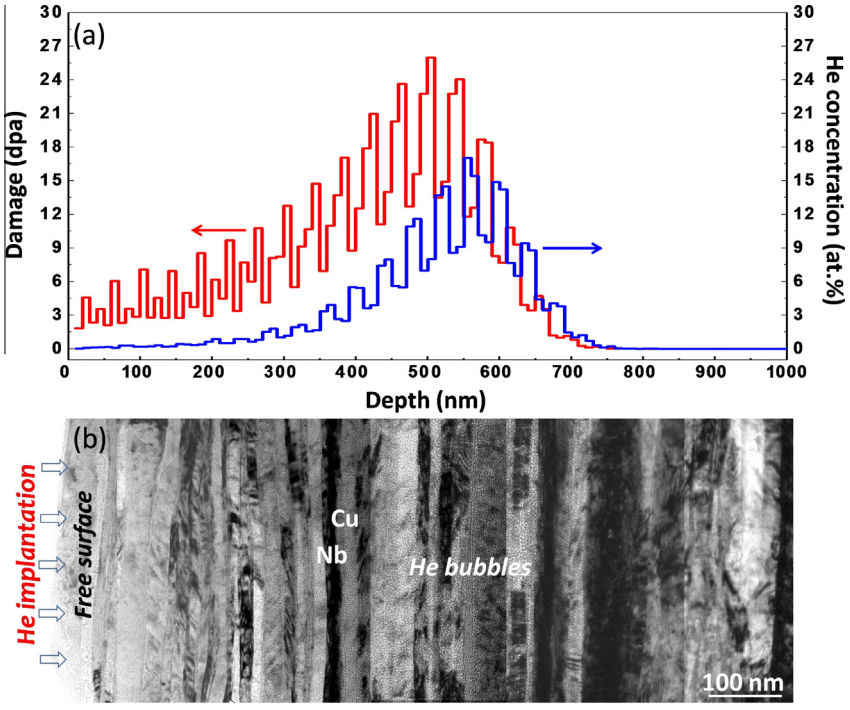

Fig. 1. (a) He concentration and displacement damage computed using SRIM and plotted as a function of depth beneath the free surface in ARB Cu–Nb irradiated by 200 keV He irons with a dose of 2×10^{21} ions/m^2; (b) XTEM image, −3 μm defocus, of ARB Cu–Nb composites with 20 nm average layer thickness after He implantation at 20 °C.

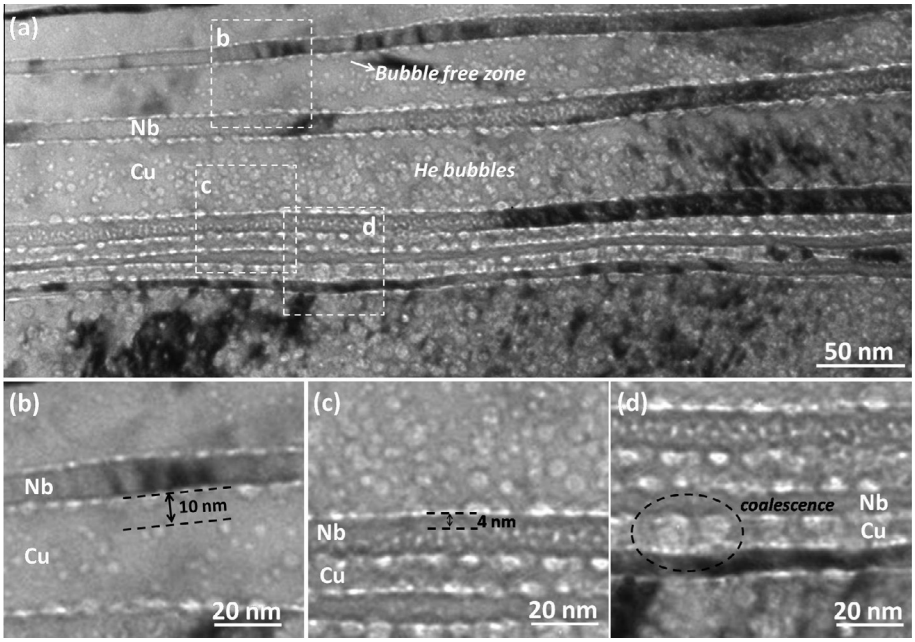

Fig. 3. (a) XTEM image, −1 μm defocus, of the region with peak He concentration in ARB Cu–Nb composites implanted with He at 450 °C (b) and (c) show zones denuded of He bubbles (d) shows coalescence of bubbles from opposite sides of a Cu layer.

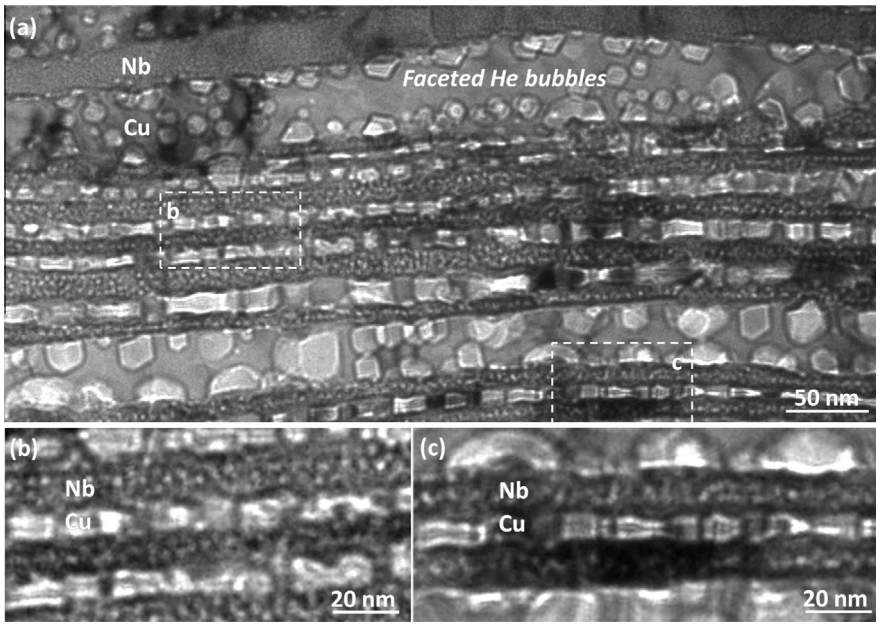

Fig. 4. (a) XTEM image, −1 μm defocus, of the region with peak He concentration in ARB Cu–Nb composites implanted with He at 480 °C (b) and (c) show elongated cavities in thin Cu layers.

differences between these investigations and our study, including microstructure and composition, total implanted He, He-to-dpa ratio, and implantation procedure. All of these differences may influence the conditions for the faceting transition and require further investigation to understand fully.

As in the 450 °C implantations, implantation at 480 °C results in the coalescence of cavities growing from opposite sides of thin Cu layers. This process gives rise to elongated cavities, such as those boxed in Fig. 4(a) and shown close-up in Fig. 4(b) and (c). The coalescence of cavities in the thinner Cu layers is confined by the neighboring Nb layers and therefore gives rise to more highly elongated cavities. Remarkably, even the extensive growth of such high aspect ratio cavities does not degrade the layered morphology of the composites. For example, there is no evidence of any successive Nb layers forming bridges across thin Cu layers, causing them to pinch off. Layer pinch off initiates spherodization of layered composites under high temperature annealing [27–29] or heavy ion irradiation [30]. He precipitate sizes in Nb after implantation at 480 °C remain in the nanometer range, as at lower implantation temperatures. This phenomenon is expected since vacancy formation and migration energies are about twice as high in Nb than in Cu [18]. Therefore, He bubbles in Nb are similar at 480 °C as in implantations performed at room temperature.

The results of the investigations described above are also summarized in Table 1. Comparing these results with previous investigations [1–7], we find that the behavior of bulk ARB Cu–Nb

Table 1
Summary of He-induced microstructure characteristics in ARB Cu–Nb composites as a function of He implantation temperature.

Implantation temperature (°C)	20	450	480
He-filled cavity size in Nb (nm)	~2	~2	~2
He-filled cavity size in Cu (nm)	~2	~5 (in layers), ~7 (at interfaces)	12–24
He-filled cavity shape in Cu (nm)	Spherical	Spherical	Faceted
Coalescence of cavities in Cu into elongated channels	No	Yes	Yes

nanocomposites under He implantation is qualitatively similar to that of magnetron sputtered Cu–Nb composites. In both cases, interfaces are good He trapping sites and interfacial He precipitates grow preferentially into Cu layers. At elevated temperatures, He bubbles in Cu transform into larger, faceted voids while He precipitates in Nb layers remain in the nanometer regime. In both ARB Cu–Nb and magnetron sputtered Cu–Nb, cavities may coalesce to form elongated channels confined to thin Cu layers by the neighboring Nb. Remarkably, even such dramatic He-induced microstructures do not destabilize the layered composite morphology. Layered nanocomposites fabricated by ARB are therefore intriguing materials for further study in environments where materials experience copious He implantation during service.

4. Conclusion

We studied the He implantation behavior of bulk ARB Cu–Nb nanocomposites. Nanoscale He precipitates form preferentially along Cu–Nb interfaces during implantation at 20 °C and 450 °C. Bubble-free zones may be identified near interfaces after implantation at 450 °C. He implantation at 480 °C results in large, faceted cavities in thick Cu layers and highly elongated cavities in thin Cu layers. In contrast, only nanoscale bubbles are seen in Nb layers after implantation up to 480 °C. The change in cavity shape in Cu layers from spherical at 450 °C to faceted at 480 °C may be an indication of bubble-to-void transition and requires further study. Bulk Cu–Nb nanocomposites exhibit He precipitate morphologies that are highly sensitive to implantation temperature and layer thickness.

Acknowledgements

This work was supported by the Center for Materials in Irradiation and Mechanical Extremes (CMIME), an Energy Frontier Research Center (EFRC) funded by the US Department of Energy, Office of Science, Office of Basic Energy Sciences under Award No. 2008LANL1026. WZH was partially supported by the new faculty start-up funding from XJTU, China. WZH also acknowledges I.J. Beyerlein for fruitful discussion as well as E.G. Fu and J. Zhang for their assistance with the He implantation.

References

[1] T. Hochbauer, A. Misra, K. Hattar, R.G. Hoagland, J. Appl. Phys. 98 (2005) 123516.
[2] X. Zhang, N. Li, O. Anderoglu, H. Wang, J.G. Swadener, T. Hochbauer, A. Misra, R.G. Hoagland, Nucl. Instrum. Methods Phys. Res. Sect. B 261 (2007) 1129.
[3] A. Misra, M.J. Demkowicz, X. Zhang, R.G. Hoagland, Jom 59 (2007) 62.
[4] M.J. Demkowicz, D. Bhattacharyya, I. Usov, Y.Q. Wang, M. Nastasi, A. Misra, Appl. Phys. Lett. 97 (2010) 161903.
[5] K. Hattar, M.J. Demkowicz, A. Misra, I.M. Robertson, R.G. Hoagland, Scr. Mater. 58 (2008) 541.
[6] M.J. Demkowicz, Y.Q. Wang, R.G. Hoagland, O. Anderoglu, Nucl. Instrum. Methods Phys. Res., Sect. B 261 (2007) 524.
[7] M. Zhernenkov, M.S. Jablin, A. Misra, M. Nastasi, Y.-Q. Wang, M.J. Demkowicz, J.K. Baldwin, J. Majewski, Appl. Phys. Lett. 98 (2011) 241913.
[8] X. Zhang, E.G. Fu, A. Misra, M.J. Demkowicz, Jom 62 (2010) 75.
[9] E.G. Fu, A. Misra, H. Wang, L. Shao, X. Zhang, J. Nucl. Mater. 407 (2010) 178.
[10] N. Li, J.J. Carter, A. Misra, L. Shao, H. Wang, X. Zhang, Philos. Mag. Lett. 91 (2010) 19.
[11] Q.M. Wei, Y.Q. Wang, M. Nastasi, A. Misra, Philos. Mag. 91 (2011) 553.
[12] M.J. Demkowicz, A. Misra, A. Caro, Curr. Opin. Solid State Mater. Sci. 16 (2012) 101.
[13] A. Kashinath, P. Wang, J. Majewski, J.K. Baldwin, Y.Q. Wang, M.J. Demkowicz, J. Appl. Phys. 114 (2013) 043505.
[14] D. Bhattacharyya, M.J. Demkowicz, Y.Q. Wang, R.E. Baumer, M. Nastasi, A. Misra, Microsc. Microanal. 18 (2012) 152.
[15] A. Kashinath, A. Misra, M.J. Demkowicz, Phys. Rev. Lett. 110 (2013) 086101.
[16] A. Kashinath, M.J. Demkowicz, Model. Simul. Mater. Sci. Eng. 19 (2011) 035007.
[17] N. Li, M. Nastasi, A. Misra, Int. J. Plast. 32–33 (2012) 1.
[18] W.Z. Han, M.J. Demkowicz, N.A. Mara, E.G. Fu, S. Sinha, A.D. Rollett, Y.Q. Wang, J.S. Carpenter, I.J. Beyerlein, A. Misra, Adv. Mater. 25 (2013) 6975.
[19] W.Z. Han, J.S. Carpenter, J. Wang, I.J. Beyerlein, N.A. Mara, Appl. Phys. Lett. 100 (2012) 011911.
[20] I.J. Beyerlein, N.A. Mara, J. Wang, J.S. Carpenter, S.J. Zheng, W.Z. Han, R.F. Zhang, K. Kang, T. Nizolek, T.M. Pollock, Jom 64 (2012) 1192.
[21] S.J. Zheng, I.J. Beyerlein, J.S. Carpenter, K.W. Kang, J. Wang, W.Z. Han, N.A. Mara, Nat. Commun. 4 (2013) 1696.
[22] S.B. Lee, J.E. LeDonne, S.C.V. Lim, I.J. Beyerlein, A.D. Rollett, Acta Mater. 60 (2012) 1747.
[23] G.J.C. Carpenter, R.B. Nicholson, High-temperature embrittlement of metals by rare gas bubbles, in: Radiation Damage in Reactor Materials, IAEA, Vienna, 1969, pp. 383–400.
[24] S.J. Zinkle, K. Farrell, H. Kanazawa, J Nucl. Mater. 179–181 (1991) 994–997.
[25] L.K. Mansur, W.A. Coghlan, J. Nucl. Mater. 119 (1983) 1.
[26] R.E. Stoller, G.R. Odette, J. Nucl. Mater. 131 (1985) 118.
[27] A. Misra, R.G. Hoagland, J. Mater. Res. 20 (2005) 2046.
[28] J. Wang, P.M. Anderson, Acta Mater. 53 (2005) 5089.
[29] P.M. Anderson, J. Wang, S. Narayanaswamy, Mater. Res. Soc. 854 (2004) U7.4.1.
[30] L. Zhang, M.J. Demkowicz, Appl. Phys. Lett. 103 (2013) 061604.